THE JOURNAL OF PHYSICAL CHEMISTRY LETTERS
A JOURNAL OF THE AMERICAN CHEMICAL SOCIETY

pubs.acs.org/JPCL

Letter

Enhanced Higher Harmonic Generation in Modified $MAPbBr_{3-x}Cl_x$ Single Crystal by Additive Engineering

Sarvani Jowhar Khanam, Srinivasa Rao Konda,* Ravi Ketavath, Wufeng Fu, Wei Li,* and Banavoth Murali*

Cite This: *J. Phys. Chem. Lett.* 2023, 14, 9222−9229

Read Online

ACCESS | Metrics & More | Article Recommendations | Supporting Information

ABSTRACT: Mixed-halide perovskite materials (MHSCs) hold significant interest in photonics applications owing to their inherent advantages, including tunable bandgap properties, remarkable defect tolerance characteristics, and facile processability. These attributes position MHSCs as up-and-coming materials for various applications. However, the commercialization of these materials is severely affected by external factors, such as humidity and oxygen. The current work studies change in higher harmonics generation (HHG) in $MAPbBr_{3-x}Cl_x$ single crystals (MHSC) with changing nitrogen-based additives. These additives act as a passivating layer and improve the nanolevel crystallinity. The additive engineering strategy impacts morphological and optical properties, depending on the additive's interaction.

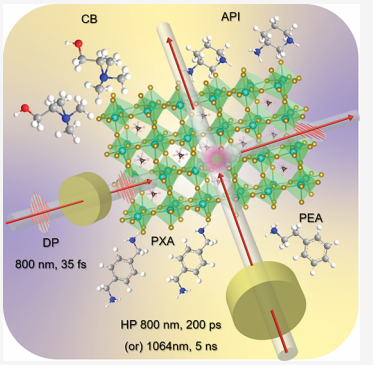

Organic−inorganic hybrid mixed-halide perovskite single crystals (PSCs) are auspicious resources in nearly all fields of science and technology, such as light-emitting diodes,[1,2] lasers,[3,4] luminescent solar concentrators,[5,6] memristors,[7] photovoltaics,[8] X-rays,[9] and γ rays owing to these materials' tunable bandgaps and higher optoelectronic properties with a large dielectric constant and low-cost processability.[10,11] Perovskite materials possess an ABX_3 structure in which a bandgap is formed by combining the metal and halide (MX_6, octahedral unit) *s*, *p* orbitals. Changing the concentration of halides and metals can directly influence bandgap tuning. Cations located in the voids of these interlinked octahedra indirectly affect these materials' bandgap.[12]

Crystals are grown either by optimizing the material composition or by optimizing the temperature. Some crystallization methods include the inverse temperature method (ITC),[13] temperature-lowering method,[14] top-seeded crystallization method,[15] antisolvent vapor assistant method (AVC),[16] Bridgman growth method,[17] low-temperature gradient crystallization,[18] cavitations triggered asymmetrical crystallization, and room-temperature liquid diffused separation induced crystallization (LDSC).[19] Although PSC growth techniques have rapidly improved the surface quality[20,21] and crystals' performance, stability issues like phase segregation,[22−24] rapid material degradation,[25,26] hysteresis,[27,28] and environmental factors such as moisture and heat are the challenges that hamper the commercialization of these materials.[29,30]

Phase segregation has been explained by using a continuous wave (CW) diode laser in the case of microcrystalline thin films. Additionally, forming formamidinium and cesium lead iodide solid-state alloys stabilized the perovskite structures by tuning the tolerance factor.[24] Doping of Cl into perovskite precursor solutions has been widely reported to tune the optoelectronic properties of perovskite materials.[31,32] Meanwhile, a traditional class of $MAPbBr_{3-x}Cl_x$ (x = 0 to 3) SCs at different concentrations of Cl doping has been investigated by Mix et al. with increased LED performances in the case of x = 0.06 (2% Cl).[32] In a recent study, using laser-induced plasma plumes (LIPs) from $MAPbBr_3$ SCs with changing additives led to the exploration of high-order nonlinear properties through higher harmonics generation (HHG).[33] The study demonstrated a change in HHG with different additives' interactions. However, only a few reports are available in the literature on the additive engineering strategy for 3D MHSC growth and its tunable HHG. Perovskite-based HHG faces several key challenges. These include stability against environmental factors, precise bandgap control for desired photon energy, understanding and optimizing nonlinear optical (NLO) responses, improving conversion efficiencies, achieving phase matching in complex structures, and addressing technical requirements for generating high-intensity laser pulses. Additionally, integration with existing technologies, developing

Received: September 1, 2023
Accepted: October 2, 2023
Published: October 9, 2023

https://doi.org/10.1021/acs.jpclett.3c02454
J. Phys. Chem. Lett. 2023, 14, 9222−9229

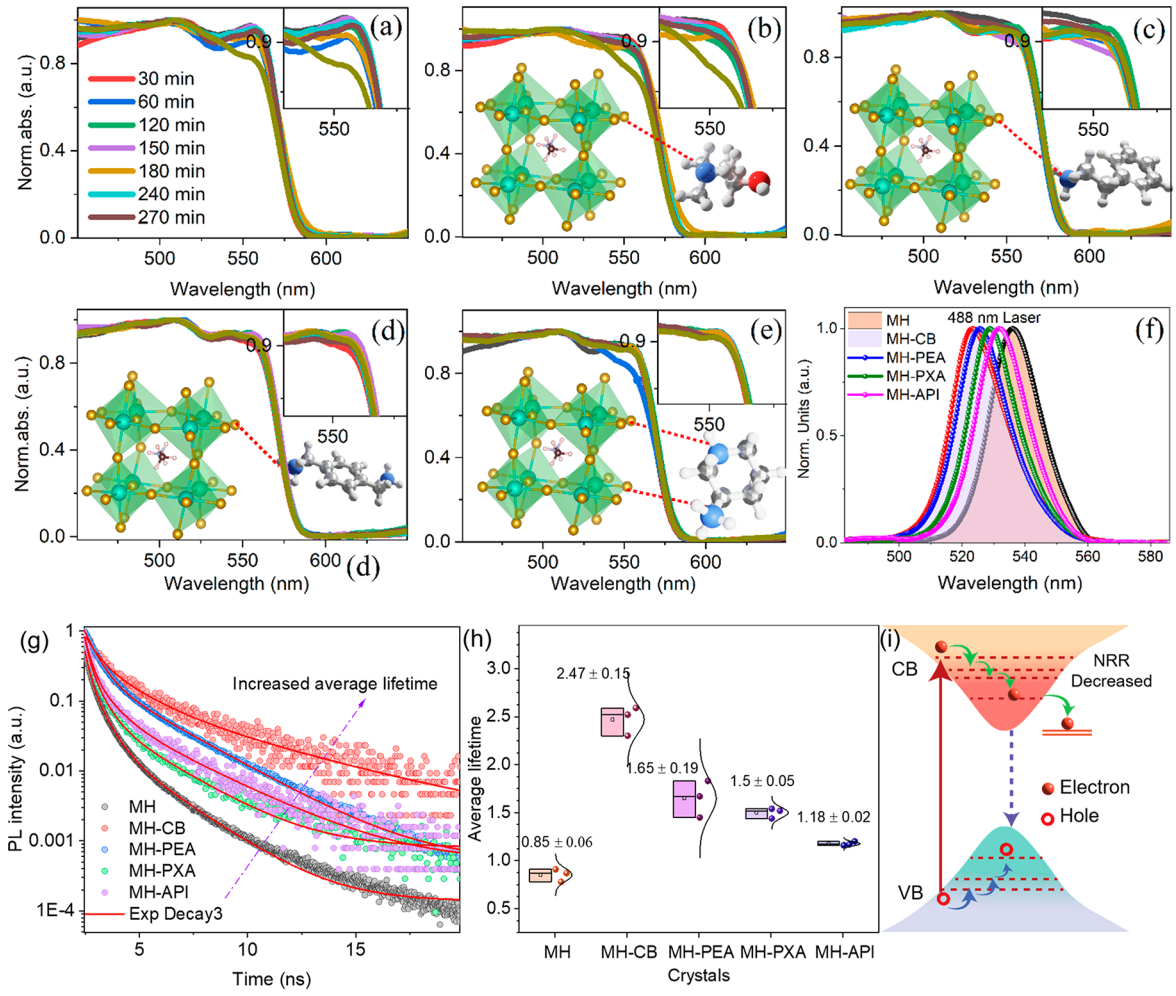

Figure 1. (a–e) Surface degradation of SCs in the outer atmosphere at a constant 60 °C temperature at different time intervals has been studied using UV spectroscopy. (f) PL spectra recorded with a 488 nm laser. (g) Average lifetime of MHPSCs with changing additives. (h) Distribution box plot represents the MHSCs repeated experimental values of TRPL. (i) Schematic representation of decreasing surface defects by adding additives to electronic band structure model in modified MHPSCs compared to pristine samples.

accurate measurement techniques, and understanding fundamental processes are crucial for advancing this technology's practical applications in ultrafast lasers. Overcoming these challenges is essential for fully realizing the potential of perovskite-based HHG. In this work, change in HHG with different additives has been studied by considering the promising composition of 6.67% Cl-doped MHSCs (owing to outperforming optoelectronic properties with low Cl fraction, with a bandgap of 2.3 eV were reported elsewhere).[32] Additives form an ionic interaction with the crystallites in a solution that can modify the nucleation and prevent preferential directional growth and crystal growth dynamics, which impact the HHG. Fundamental characterizations were done in our recently published article. This Letter addresses changes in thermal stability, and tunable HHG of MHPSCs was studied using 800 nm and 35 fs as the driving pulse (DP) and heating pulses (HP) of 800 nm, 200 ps and 1064 nm, 6 ns by taking the choline bromide (CB), phenylethylamine hydrochloride (PEA), P-xylylenediamine dihydrochloride (PXA), and (R)-3-aminopiperidine dihydrochloride (API) to $MAPbBr_{2.8}Cl_{0.2}$ SC (pristine) in the precursor solution to grow MH-CB, MH-PEA, MH-PXA, and MH-API.

N-based aliphatic, aromatic with one or two amine groups, and heterocyclic organic molecules as an additive interact differently with the surface and have higher stability than their MABr counterparts.[33] In the present work, we have chosen salts of additives such as CB, aliphatic; PEA, aromatic; PXA, aromatic; and API, heterocyclic to grow the $MAPbBr_{2.8}Cl_{0.2}$ SC (MH, pristine), which acts as a passive layer on the surface of MHSCs. Changes in absorbance values representing surface degradation of SCs in the outer atmosphere at a constant 60 °C temperature at different time intervals have been studied using ultraviolet–visible (UV) spectroscopy (panels a–e of Figure 1). The photoluminescence (PL) measurements using a 488 nm laser observed a blue shift as the Cl concentration increased in the modified MHSCs, as shown in Figure 1f. Most of the literature showed that the bandgap of perovskite crystals increases after adding a small amount of Cl ions.[32] However, a decrease in halide vacancies and incorporation of Cl might be attributed to a change in the PL of the modified crystals.[32]

Generally, the transient evolution of the electron–hole population after impulsive photoexcitation can be calculated from time-resolved PL (TRPL) measurements. Herein, the changes in average exciton lifetime are investigated using TRPL. Subsequently, the decay curves of the excited carrier in the modified PSCs are fitted using a triexponential decay model to quantify the carrier dynamics, and the fitted parameters are summarized in Table 1.[33−35] The average PL

https://doi.org/10.1021/acs.jpclett.3c02454
J. Phys. Chem. Lett. 2023, 14, 9222−9229

Table 1. Comparative Study of the MHPSCs Thermodynamic Properties of Phase One Transformations

MHPSCs	Temperature (T_s) °C	E_a (kJ mol^{-1})	ΔHs (kJ/g)	ΔS (J/g °C)	ΔG (kJ mol^{-1})
MH	328.69	177.93	172.43	−32.14	193.70
MH-CB	329.52	127.98	122.39	−104.99	192.93
MH-PEA	328.70	169.77	164.20	−46.299	195.23
MH-PXA	328.97	183.79	178.34	−20.251	191.62
MH-API	328.69	168.19	162.61	−49.259	195.69

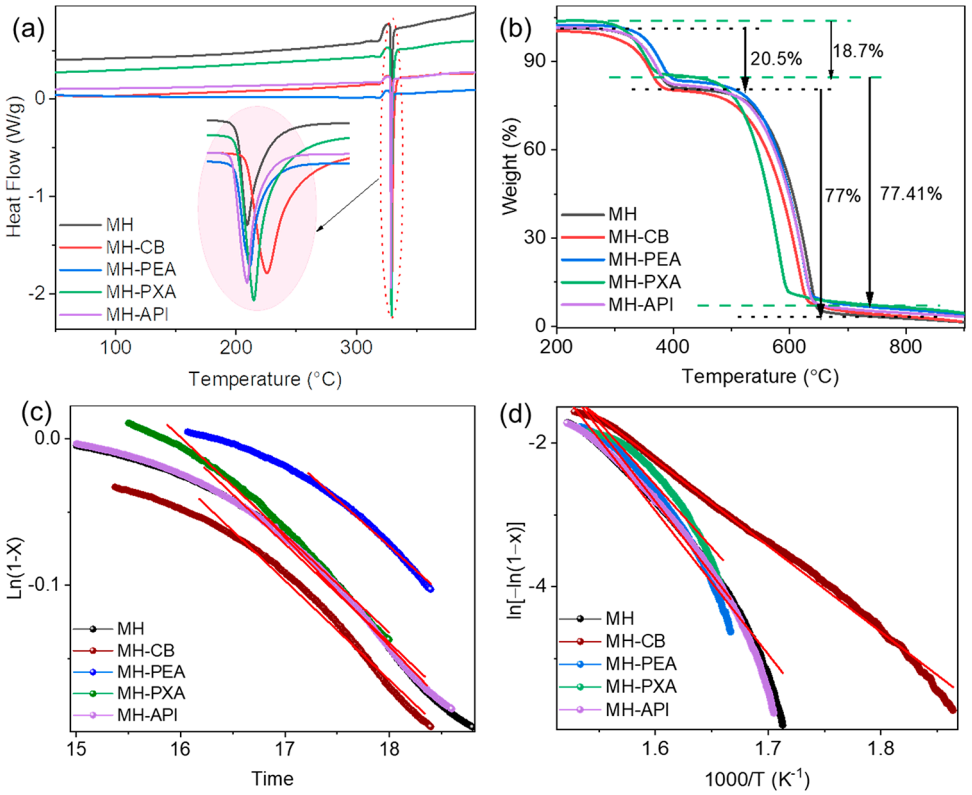

Figure 2. (a) Change in phase transition temperature (inset) second heating in differential scanning calorimetry. (b) TGA of pristine and modified MHPSCs. (c, d) Plots of $\ln(1 - x)$ vs time and $\ln[-\ln(1 - x)]$ vs $1000/T$ of organic moiety decomposition in MHPSCs.

lifetime considerably increased in modified MHSCs compared to pristine ones (Figure 1g). Figure 1h illustrates a distribution box plot representing the MHSC's repeated experimental values of TRPL. Based on the evidence gathered from various optical measurements, it can be inferred that the reduction of surface defects proceeds through the incorporation of additives. The electronic band structure model in modified MHPSCs is schematically represented in Figure 1i. In some cases, the decay curves of the excited carrier in the modified PSCs were fitted using a triexponential decay model to quantify the carrier dynamics.[33] The relatively faster decay components (τ_1 and τ_2) are attributed to charge carrier trapping defect states, while the slower decay components (τ_3) are assigned to radiative recombination in the bulk material. The average PL lifetime was significantly enhanced from 0.85 to 2.47 ns, suggesting that the additives lengthen the charge carrier lifetimes within the bulk crystal. Photographs of MH, MH-CB, MH-PEA, MH-PXA, and MH-API are given in Figure S1 of the Supporting Information.

The thermodynamic properties in modified MHPSCs have been anlyzed by using differential scanning calorimetry (DSC) and thermogravimetric analysis (TGA) with a heating rate of 10 °C/min in an N_2 atmosphere. Interestingly, a change in the phase transition temperature (T_s) in modified MHPSCs was observed around 328.69 to 329.52 °C in DSC. Subsequently, it indicates whether the process is exothermic or endothermic, as shown in Figure 2a. Most PSCs' thermal decomposition follows two steps, first organic moiety and second lead halide decomposition in TGA, as shown in eq 1.[36]

$$CH_3NH_3PbX_3 \xrightarrow[\Delta]{X=Cl/Br} CH_3{-}NH_2 + HX + PbX_2 \quad (1)$$

TGA of pristine and modified MH-PXA SCs has shown a decomposition with weight losses of 22.7%, 73.41%, and 20.8, 66% at each step, respectively (Figure 2b). Herein, the organic moiety degradation starts at ∼300 and ends at 382 °C. Considering phase transformations as first-order reactions, the kinetics and thermodynamic parameters of the reaction were calculated using the equations reported in the literature.[37]

$$\frac{dx}{dt} = k(1 - x) \quad (2)$$

where

$$x = \frac{w_i - w_t}{w_i - w_f} \quad (3)$$

https://doi.org/10.1021/acs.jpclett.3c02454
J. Phys. Chem. Lett. 2023, 14, 9222−9229

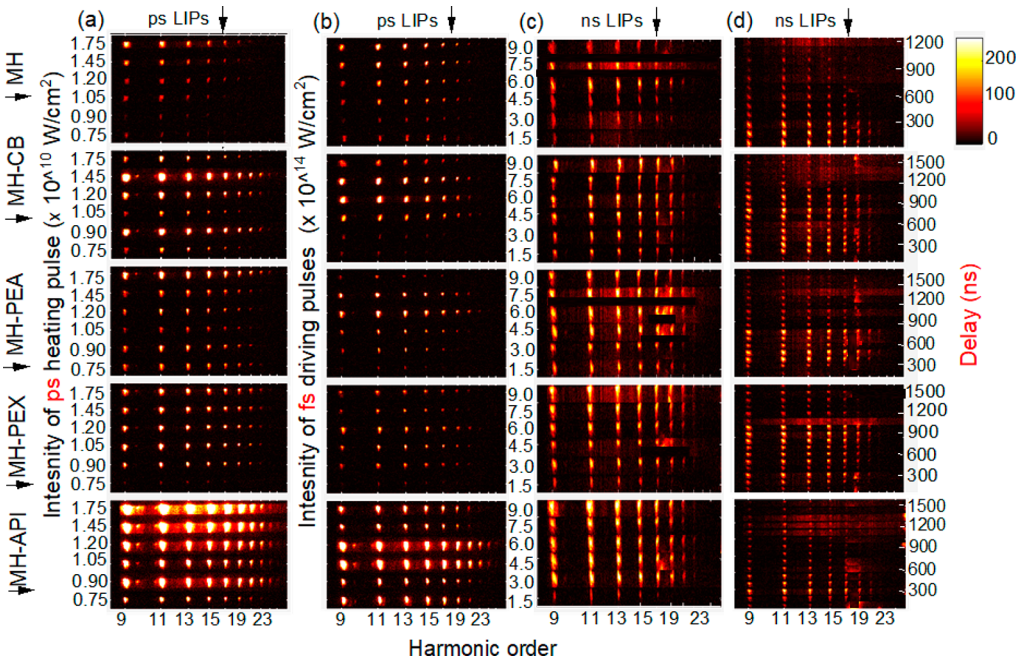

Figure 3. Harmonic spectra (in pixels) for different (a) ps heating pulse intensities at $I_{fs} = 6 \times 10^{14}$ W/cm^2. (b and c) Driving pulse intensities for ps LIPs (at $I_{ps} = 0.9 \times 10^{10}$ W/cm^2) and ns LIPs ($I_{ns} = 7 \times 10^{10}$ W/cm^2), respectively. (d) The delay dependence between ns HP and fs DPs. The spectrum's color bar is similar in the top right corner.

w_i is the initial weight, w_t is the weight of the sample at a particular time t, and w_f is the final weight. A straight line of a plotted graph (Figure 2c) using eqs 2 and 3 for the selected phase confirms the first-order reactions. Kinetics parameters were determined using a modified form of the Coats and Redfern model, as described in eq 4.

$$\ln[-\ln(1-x)] = \ln\frac{ART^2}{\beta E_a} - \frac{E_a}{RT} \tag{4}$$

where A is the pre-exponential factor, β is a heating rate (10 °C/min), R is the general gas constant (8.3143 J mol^{-1} K^{-1}), E_a is activation energy, and T is the temperature (K).

Activation energy (E_a) values are extracted from the slope of the $\ln[-\ln(1-x)]$ vs $1000/T$ plot (Figure 2d). Furthermore, changes in entropy (ΔS), enthalpy (ΔH), and Gibbs free energy (ΔG) were determined using basic thermodynamic equations.[37] Resulting values obtained for phase one and phase two are plotted in Figure S2 of the Supporting Information, and phase one values are presented in Table 1. Herein, positive values of ΔH and ΔG show that the decomposition of the organic moiety is a nonspontaneous reaction. From overall thermodynamic parameters, it could be concluded that MH-CB SCs have relatively higher thermal stability than the pristine ones. The enhanced thermal stability of the modified crystal can be attributed to its increased interactions of additives with the crystal surface. Moreover, our results are close to previous observations in the literature.[38,39]

Recently, high-order nonlinear properties using HHG in LIPs of Ni-doped $CsPbBr_3$ 2D colloidal nanocrystals have been researched, and the improvement of harmonics was determined for optimized % of Ni.[40−43] Harmonic spectra of modified crystals were obtained as stacks illustrated in panels a−d of Figure 3. In the first step, (a) at DP intensity, i.e., 6×10^{14} W/cm^2, we measured the harmonic spectra by changing the ps HP intensities. All the samples emitted the harmonics at lower ps HP intensity (I_{ps}) of 0.75×10^{10} W/cm^2. The harmonics intensity and cutoff were significantly improved with a further increase in the I_{ps} up to 1.77×10^{10} W/cm^2. Notably, at low I_{ps} for the MH obtained, the harmonics cutoff was up to 13H, whereas for additive-based SCs, the cutoff was extended to 19H. This indicates that the plasma plume density was enhanced in the case of additives in comparison to MH. In the second and third steps (b and c), we measured the harmonics spectra individually at fixed ps and ns HP intensities, i.e., 0.9 and 7×10^{10} W/cm^2, and varied the DP intensity (I_{fs}) between 1.5 and 9×10^{10} W/cm^2. In the case of picosecond LIPs, the cutoff achieved up to 19H (MH) and 21H (MH-CB, MH-PEA, and MH-PEX). In contrast, it is increased up to 25H for MH-API. However, in the case of ns LIPs, the cutoff is similar for all the crystals, i.e., up to 21H.

In the fourth step (d), we fixed the ns HP intensity (I_{ns}) at 7×10^{10} W/cm^2 and measured the harmonic spectra concerning the delay between ns HP and fs DPs. In the case of nanosecond LIPs, either variation in I_{fs} or change in the delay, we could not observe much difference in the harmonic cutoff. However, the intensity of the harmonics is improved for additive-based crystals at longer delays, as shown in Figure 3d. The cutoff delays were achieved at 1200 ns for MH, while for MH-CB, MH-PEA, and MH-API it is similar to around 1600 ns, whereas for MH-API, it is up to 1500 ns.

MA shows the first maxima at a 100 ns delay within these delay ranges, continuously decreasing the harmonic intensity and having peaks at every 200 ns, whereas MH-PEX and MH-API exhibit 300 ns. The modified SCs also show a similar trend to MH, while all their peaks appear at each 200 ns delay. This indicates the ejection of plasma components, such as atoms, ions, and nanoparticles with different masses. The DP is propagating above the target surface at approximately a 0.2 mm distance. Meanwhile, it is observed that the harmonics emitted for additive SCs show a shift compared to MH. Panels e and f of Figure 4 show the normalized intensity of 9H in the case of ns and ps LIPs, respectively. The shift in ps LIPs is

https://doi.org/10.1021/acs.jpclett.3c02454
J. Phys. Chem. Lett. 2023, 14, 9222−9229

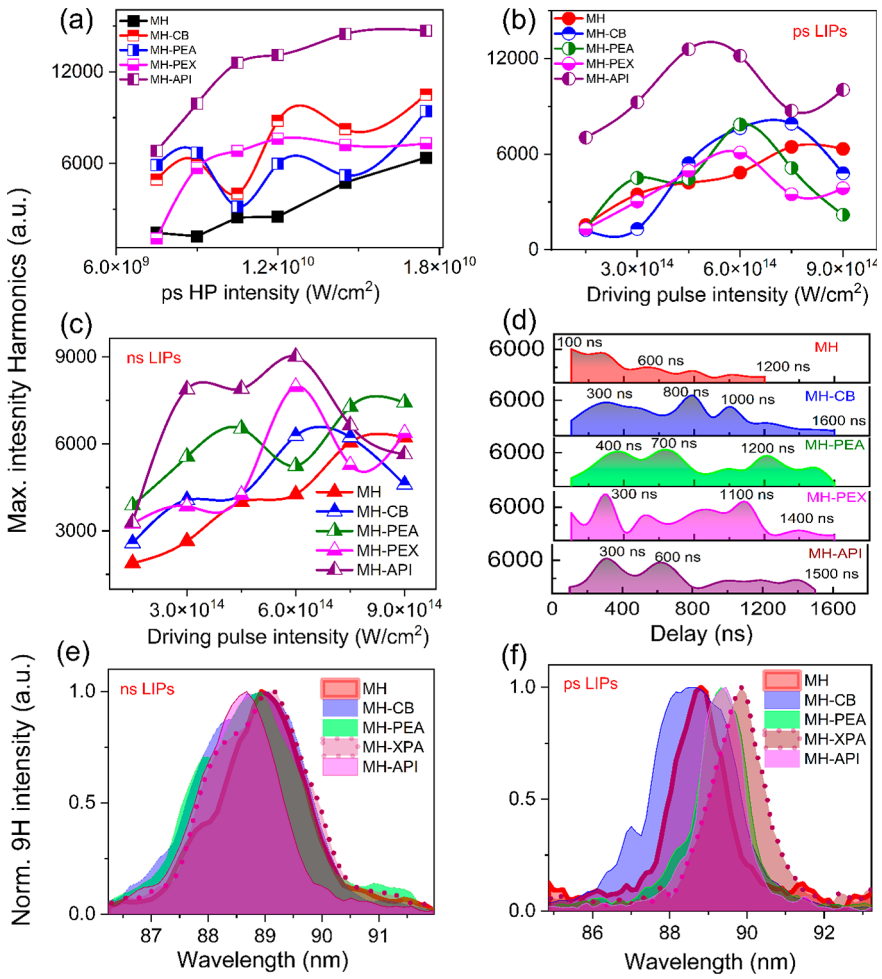

Figure 4. Maximum harmonic signal for different (a–c) ps heating pulse intensities at $I_{fs} = 6.0 \times 10^{14}$ W/cm^2, driving pulse intensities for ps LIPs (at $I_{ps} = 0.9\times 10^{10}$ W/cm^2), and ns LIPs ($I_{ns} = 7 \times 10^{10}$ W/cm^2), respectively. (d) The delay dependence between ns HP and fs DPs. (e and f) The shift of 9H for all SCs in the case of ns LIPs and ps LIPs.

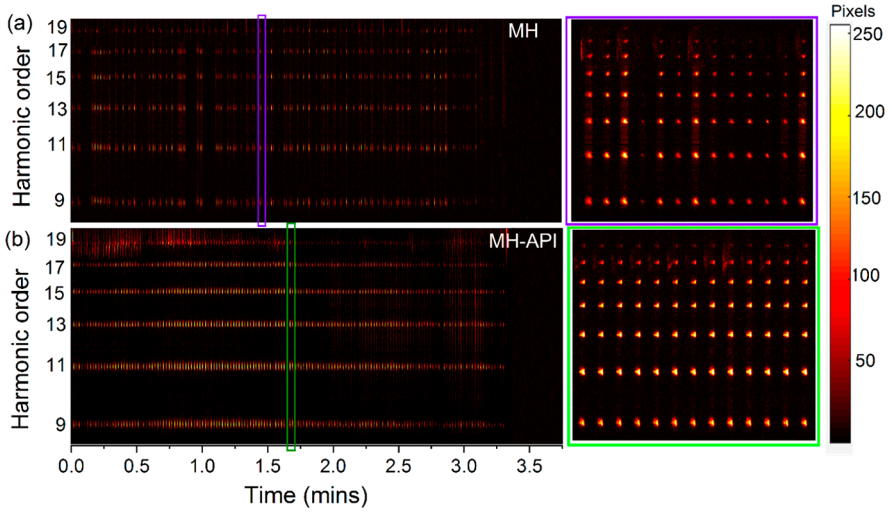

Figure 5. Harmonic spectra of (a and b) MH and MH-API with respect to time. The harmonic spectra were recorded as movies and plotted as vertical stack images. The right portion of panels a and b represents the region marked with pink and green lines, respectively.

much higher than the ns LIPs. In the case of ns LIPs, the MH-CB, MH-PEA, and MH-API show a bluer shift, whereas MH-PXA shows a redshift in both cases of plasma plumes. The DP we have used is 800 nm, and in the case of ns pulses, we used 1064 nm as an ablating laser pulse, and for ps pulses, the wavelength is the same as the DP. Nonlinear absorption of MHPSCs at 800 nm emits PL radiation and ejection of plasma components during laser ablation. At the same time, only

https://doi.org/10.1021/acs.jpclett.3c02454
J. Phys. Chem. Lett. 2023, 14, 9222–9229

plasma plume formation is achieved in the case of ns laser ablation. Therefore, it is assumed that the plasma components (atoms, ions, and nanoparticles) of modified MHPSCs with low/higher bandgaps might interact with the blue/red spectral components of 800 nm and decrease/increase the wavelengths of the harmonics. Moreover, as discussed, the order of PL emission intensity follows the order MH > MH-PEA > MH-PXA > MH-CB > MH-API; this order is reversed in the case of harmonics intensity, as appears in panels a−c of Figure 4. This confirms that at probing of 800 nm, the MHPSCs lead to higher absorption and principal PL emission (either by ablation of picosecond and nanosecond pulses) and decrease the intensity of the harmonics compared to the modified MHPSCs. The MH-CB and MH-PEA SCs have first maxima around 800 ns and 700 ns.

In addition, we measured the harmonic spectra continuously until the disappearance of harmonic signal from SC plasma plumes. Panels a and b of Figure 5 depict the harmonic spectra of MH and MH-API as a function of time. The plasma plumes are produced by nanosecond heating pulses at a fixed position of the crystal surface, and the harmonic spectra have been recorded as a movie using CCD. Each frame harmonics spectra are plotted as a vertical stack image. It is observed that the MH crystal emits harmonics for 3.15 min, and the modified MHPSCs exceed this time duration. For example, the MH-API (shown in Figure 5b) emits the harmonic signal for up to 3.35 min. Approximately a similar time was achieved for MH-CB, MH-PEA, and MH-PEX. Therefore, one can assume that the additives increased the stability of crystals. Overall, the measured harmonics spectra, either picosecond or nanosecond LIPs from these SCs, the additives increased the stability of crystals further, which leads to the intensity enhancement and the shift in the harmonics. Among all reported SCs, MA-API has a higher intensity than others, and in the case of ps LIPs, MH-PXA shows a larger redshift (for 9H, $\Delta\lambda$ = +1.05 nm). The HHG studies with various laser parameters, such as intensities of DP, HP, and delay dependence between DP and HP, revealed that the additive-based SCs enhanced the emission of harmonics in the extreme ultraviolet (XUV) region more than pristine MHPSCs.

As discussed above, our previous study on $MAPbBr_3$ SCs with changing additives demonstrated a change in HHG with different additives' interactions.[33] In the current investigation, an increase in the Cl percentage led to an increase in the high-harmonic generation (HHG) cutoff. It is well-known that HHG is a three-step model: (i) ionization by an intense laser field, (ii) acceleration in the laser field, and (iii) recombination with the parent ion, leading to the generation of high-energy photons. It has been observed that the MH crystal emits the harmonics until 3.15 min, and the modified MHPSCs exceed this time duration up to 3.35 min (shown in Figure 5b). In contrast, pristine $MAPbBr_3$ continuously produced plasma plumes for 2.66 min as the first ionization potential Cl is greater than the Br. Due to this, the plasma density (containing atoms and singly charged ions) will be higher in the case of MH PSCs than MA. This is also supported by the harmonic emission from MA and MH crystals concerning ps LIPs. Figure S4 of the Supporting Information compares harmonic intensity emitted from MA and MH crystals with respect to driving pulse intensities. Even in the case of the MA crystal, the ablating ps intensity is twice that of the MH crystal at low and high DP intensities, *i.e.*, 1.5 and 9.0 × 10^{14} W/cm^2, and the MH crystal shows higher intensities than the MA crystal, which confirms that MH crystals possess denser plasma components than MA crystals.

In summary, we have successfully demonstrated an additive engineering strategy for mitigating the mixed halide phase segregation effect of 6.67% Cl-doped MHSCs with additives. Out of all the additives we have observed, a bluer shift in PL emission for MH-PXA SC when excited with a 2PA source laser indicates more nonradiative recombination. Interestingly, we observed increased crystallinity with mitigated phase separation. The heterocyclic amine (API) coordination with crystallite facets resulted in enhanced harmonic emission and stability. From the overall basic characterization and HHG observations, it is estimated that additives' interaction with the surface plays an essential role in passivation along with Cl incorporated into the perovskite lattice with decreasing halide vacancies rather than being sacrificed as a volatile phase. The lattice constant of the API-MHSCs is higher than those of other additives, suggesting increased Schottky order and transparency in the bulk perovskite. This explanation is consistent with the increased interaction between the formation of MHPSCs, with API additives being more thermodynamically preferred than other additives. The present work will open the doors for tuning the higher-order harmonics' wavelength without changing the driving pulse's chirps, i.e., either positive or negative. Interestingly, in modified MHSCs, enhanced harmonic intensity and stability have been observed. Therefore, we can conveniently use a modified MHPSC in plasma HHG with advanced properties in harmonic spectroscopic applications.

■ ASSOCIATED CONTENT

Supporting Information

The Supporting Information is available free of charge at https://pubs.acs.org/doi/10.1021/acs.jpclett.3c02454.

Experimental details of MHSCs; synthesis method; literature review and instrumental details (Table S1); comparative study of MHPSCs TRPL decay profiles (Table S2); photographs of MH, MH-CB, MH-PEA, MH-PXA, and MH-API (Figure S1); comparative study of MHPSCs thermodynamic properties (Figure S2) and X-ray diffraction pattern of the modified and pristine SCs representing the elemental ratios extracted from energy dispersive X-ray analysis data (Figure S3); comparison of harmonic intensities for $MAPbBr_3$ and MH crystals with respect to driving pulse intensity (Figures S4) (PDF)

Transparent Peer Review report available (PDF)

■ AUTHOR INFORMATION

Corresponding Authors

Srinivasa Rao Konda − *The GPL Photonics Laboratory State Key Laboratory of Luminescence and Applications, Changchun Institute of Optics Fine Mechanics and Physics, Chinese Academy of Sciences, Changchun 130033, China;* orcid.org/0000-0002-9001-4857; Email: ksrao@ciomp.ac.cn

Wei Li − *The GPL Photonics Laboratory State Key Laboratory of Luminescence and Applications, Changchun Institute of Optics Fine Mechanics and Physics, Chinese Academy of Sciences, Changchun 130033, China;* Email: weili1@ciomp.ac.cn

https://doi.org/10.1021/acs.jpclett.3c02454
J. Phys. Chem. Lett. 2023, 14, 9222−9229

Banavoth Murali − *Solar Cells and Photonics Research Laboratory, School of Chemistry, University of Hyderabad, Hyderabad 500046 Telangana, India;* orcid.org/0000-0002-7806-2274; Email: murali.banavoth@uohyd.ac.in

Authors

Sarvani Jowhar Khanam − *Solar Cells and Photonics Research Laboratory, School of Chemistry, University of Hyderabad, Hyderabad 500046 Telangana, India*

Ravi Ketavath − *Solar Cells and Photonics Research Laboratory, School of Chemistry, University of Hyderabad, Hyderabad 500046 Telangana, India;* orcid.org/0000-0002-1853-9210

Wufeng Fu − *The GPL Photonics Laboratory State Key Laboratory of Luminescence and Applications, Changchun Institute of Optics Fine Mechanics and Physics, Chinese Academy of Sciences, Changchun 130033, China*

Complete contact information is available at: https://pubs.acs.org/10.1021/acs.jpclett.3c02454

Notes

The authors declare no competing financial interest.

■ ACKNOWLEDGMENTS

This work is supported by the School of Chemistry, University of Hyderabad. B.M. acknowledges the Department of Science and Technology (DST) and Institute of Eminence (UOH-IOE-RC2-21-008). The Innovation Grant of Changchun Institute of Optics, Fine Mechanics and Physics (CIOMP), Jilin Provincial Science and Technology Development Project (YDZJ202102CXJD002) is acknowledged.

■ REFERENCES

(1) Vashishtha, P.; Ng, M.; Shivarudraiah, S. B.; Halpert, J. E. High-Efficiency Blue and Green Light-Emitting Diodes Using Ruddlesden−Popper Inorganic Mixed Halide Perovskites with Butylammonium Interlayers. *Chem. Mater.* **2019**, *31*, 83−89.

(2) Zhu, L.; Cao, H.; Xue, C.; Zhang, H.; Qin, M.; Wang, J.; Wen, K.; Fu, Z.; Jiang, T.; Xu, L.; Zhang, Y.; Cao, Y.; Tu, C.; Zhang, J.; Liu, D.; Zhang, G.; Kong, D.; Fan, N.; Li, G.; Yi, C.; Peng, Q.; Chang, J.; Lu, X.; Wang, N.; Huang, W.; Wang, J. Unveiling the Additive-Assisted Oriented Growth of Perovskite Crystallite for High-Performance Light-Emitting Diodes. *Nat. Commun.* **2021**, *12*, 5081.

(3) Xing, G.; Mathews, N.; Lim, S. S.; Yantara, N.; Liu, X.; Sabba, D.; Grätzel, M.; Mhaisalkar, S.; Sum, T. C. Low-Temperature Solution-Processed Wavelength-Tunable Perovskites for Lasing. *Nat. Mater.* **2014**, *13*, 476−480.

(4) Deschler, F.; Price, M.; Pathak, S.; Klintberg, L. E.; Jarausch, D. D.; Higler, R.; Hüttner, S.; Leijtens, T.; Stranks, S. D.; Snaith, H. J.; Atatüre, M.; Phillips, R. T.; Friend, R. H. High Photoluminescence Efficiency and Optically Pumped Lasing in Solution-Processed Mixed Halide Perovskite Semiconductors. *J. Phys. Chem. Lett.* **2014**, *5*, 1421−1426.

(5) Xia, P.; Xu, S.; Wang, C.; Ban, D. Perovskite Luminescent Solar Concentrators for Photovoltaics. *APL Photonics* **2021**, *6*, 120901.

(6) Fang, H. H.; Wang, F.; Adjokatse, S.; Zhao, N.; Even, J.; Loi, M. A. Photoexcitation Dynamics in Solution-Processed Formamidinium Lead Iodide Perovskite Thin Films for Solar Cell Applications. *Light Sci. Appl.* **2016**, *5*, e16056.

(7) Xing, J.; Zhao, C.; Zou, Y.; Kong, W.; Yu, Z.; Shan, Y.; Dong, Q.; Zhou, D.; Yu, W.; Guo, C. Modulating the Optical and Electrical Properties of $MAPbBr_3$ Single Crystals via Voltage Regulation Engineering and Application in Memristors. *Light Sci. Appl.* **2020**, *9*, 11.

(8) Peng, W.; Wang, L.; Murali, B.; Ho, K.-T.; Bera, A.; Cho, N.; Kang, C.-F.; Burlakov, V. M.; Pan, J.; Sinatra, L.; Ma, C.; Xu, W.; Shi, D.; Alarousu, E.; Goriely, A.; He, J.-H.; Mohammed, O. F.; Wu, T.; Bakr, O. M. Solution-Grown Monocrystalline Hybrid Perovskite Films for Hole-Transporter-Free Solar Cells. *Adv. Mater.* **2016**, *28*, 3383−3390.

(9) Bai, F.; Bian, K.; Huang, X.; Wang, Z.; Fan, H. Pressure Induced Nanoparticle Phase Behavior, Property, and Applications. *Chem. Rev.* **2019**, *119*, 7673−7717.

(10) Cho, N.; Li, F.; Turedi, B.; Sinatra, L.; Sarmah, S. P.; Parida, M. R.; Saidaminov, M. I.; Murali, B.; Burlakov, V. M.; Goriely, A.; Mohammed, O. F.; Wu, T.; Bakr, O. M. Pure Crystal Orientation and Anisotropic Charge Transport in Large-Area Hybrid Perovskite Films. *Nat. Commun.* **2016**, *7*, 13407.

(11) Murali, B.; Dey, S.; Abdelhady, A. L.; Peng, W.; Alarousu, E.; Kirmani, A. R.; Cho, N.; Sarmah, S. P.; Parida, M. R.; Saidaminov, M. I.; Zhumekenov, A. A.; Sun, J.; Alias, M. S.; Yengel, E.; Ooi, B. S.; Amassian, A.; Bakr, O. M.; Mohammed, O. F. Surface Restructuring of Hybrid Perovskite Crystals. *ACS Energy Lett.* **2016**, *1*, 1119−1126.

(12) An, Y.; Hidalgo, J.; Perini, C. A. R.; Castro-Méndez, A.-F.; Vagott, J. N.; Bairley, K.; Wang, S.; Li, X.; Correa-Baena, J.-P. Structural Stability of Formamidinium- and Cesium-Based Halide Perovskites. *ACS Energy Lett.* **2021**, *6*, 1942−1969.

(13) Khanam, S. J.; Parikh, N.; Satapathi, S.; Kalam, A.; Banavoth, M.; Yadav, P. Role of Heterocyclic Organic Compounds on the Optoelectronic Properties of Halide Perovskite Single Crystals. *ACS Appl. Energy Mater.* **2022**, *5*, 14732−14738.

(14) Dang, Y.; Liu, Y.; Sun, Y.; Yuan, D.; Liu, X.; Lu, W.; Liu, G.; Xia, H.; Tao, X. Bulk Crystal Growth of Hybrid Perovskite Material $CH_3NH_3PbI_3$. *CrystEngComm* **2015**, *17*, 665−670.

(15) Dong, Q.; et al. DigitalCommons @ University of Nebraska - Lincoln Electron-Hole Diffusion Lengths > 175 μ m in Solution-Grown $CH_3NH_3PbI_3$ Single Crystals. *Science* **2015**, *347*, 967−970.

(16) Shi, D.; Adinolfi, V.; Comin, R.; Yuan, M.; Alarousu, E.; Buin, A.; Chen, Y.; Hoogland, S.; Rothenberger, A.; Katsiev, K.; Losovyj, Y.; Zhang, X.; Dowben, P. A.; Mohammed, O. F.; Sargent, E. H.; Bakr, O. M. Low Trap-State Density and Long Carrier Diffusion in Organolead Trihalide Perovskite Single Crystals. *Science* **2015**, *347*, 519−522.

(17) Stoumpos, C. C.; Malliakas, C. D.; Peters, J. A.; Liu, Z.; Sebastian, M.; Im, J.; Chasapis, T. C.; Wibowo, A. C.; Chung, D. Y.; Freeman, A. J.; Wessels, B. W.; Kanatzidis, M. G. Crystal Growth of the Perovskite Semiconductor CsPbBr3: A New Material for High-Energy Radiation Detection. *Cryst. Growth Des.* **2013**, *13*, 2722−2727.

(18) Peng, W.; Wang, L.; Murali, B.; Ho, K. T.; Bera, A.; Cho, N.; Kang, C. F.; Burlakov, V. M.; Pan, J.; Sinatra, L.; Ma, C.; Xu, W.; Shi, D.; Alarousu, E.; Goriely, A.; He, J. H.; Mohammed, O. F.; Wu, T.; Bakr, O. M. Solution-Grown Monocrystalline Hybrid Perovskite Films for Hole-Transporter-Free Solar Cells. *Adv. Mater.* **2016**, *28*, 3383−3390.

(19) Yao, F.; Peng, J.; Li, R.; Li, W.; Gui, P.; Li, B.; Liu, C.; Tao, C.; Lin, Q.; Fang, G. Room-temperature liquid diffused separation induced crystallization for high-quality perovskite single crystals. *Nat. Commun.* **2019**, *31*, 1194.

(20) He, L.; Xiao, Z.; Yang, X.; Wu, Y.; Lian, Y.; Peng, X.; Yang, X. Green and Sky Blue Perovskite Light-Emitting Devices with a Diamine Additive. *J. Mater. Sci.* **2020**, *55*, 7691−7701.

(21) Tang, Y.; Liang, M.; Zhang, M.; Honarfar, A.; Zou, X.; Abdellah, M.; Pullerits, T.; Zheng, K.; Chi, Q. Photodetector Based on Spontaneously Grown Strongly Coupled $MAPbBr_3$/N-RGO Hybrids Showing Enhanced Performance. *ACS Appl. Mater. Interfaces* **2020**, *12*, 858−867.

(22) Knight, A. J.; Herz, L. M. Preventing Phase Segregation in Mixed-Halide Perovskites: A Perspective. *Energy Environ. Sci.* **2020**, *13*, 2024−2046.

(23) Levchuk, I.; Osvet, A.; Tang, X.; Brandl, M.; Perea, J. D.; Hoegl, F.; Matt, G. J.; Hock, R.; Batentschuk, M.; Brabec, C. J. Brightly Luminescent and Colour-Tunable Formamidinium Lead Halide Perovskite $FAPbX_3$ (X = Cl, Br, I) Colloidal Nanocrystals. *Nano Lett.* **2017**, *17*, 2765−2770.

(24) Chen, L.; Tan, Y. Y.; Chen, Z. X.; Wang, T.; Hu, S.; Nan, Z. A.; Xie, L. Q.; Hui, Y.; Huang, J. X.; Zhan, C.; Wang, S. H.; Zhou, J. Z.;

Yan, J. W.; Mao, B. W.; Tian, Z. Q. Toward Long-Term Stability: Single-Crystal Alloys of Cesium-Containing Mixed Cation and Mixed Halide Perovskite. *J. Am. Chem. Soc.* **2019**, *141*, 1665−1671.
(25) Misra, R. K.; Aharon, S.; Li, B.; Mogilyansky, D.; Visoly-Fisher, I.; Etgar, L.; Katz, E. A. Temperature- and Component-Dependent Degradation of Perovskite Photovoltaic Materials under Concentrated Sunlight. *J. Phys. Chem. Lett.* **2015**, *6*, 326−330.
(26) Niu, G.; Guo, X.; Wang, L. Review of Recent Progress in Chemical Stability of Perovskite Solar Cells. *J. Mater. Chem. A* **2015**, *3*, 8970−8980.
(27) van Reenen, S.; Kemerink, M.; Snaith, H. J. Modeling Anomalous Hysteresis in Perovskite Solar Cells. *J. Phys. Chem. Lett.* **2015**, *6*, 3808−3814.
(28) Raga, S. R.; Jung, M. C.; Lee, M. V.; Leyden, M. R.; Kato, Y.; Qi, Y. Influence of Air Annealing on High-Efficiency Planar Structure Perovskite Solar Cells. *Chem. Mater.* **2015**, *27*, 1597−1603.
(29) Yakunin, S.; Dirin, D. N.; Shynkarenko, Y.; Morad, V.; Cherniukh, I.; Nazarenko, O.; Kreil, D.; Nauser, T.; Kovalenko, M. V. Detection of Gamma Photons Using Solution-Grown Single Crystals of Hybrid Lead Halide Perovskites. *Nat. Photonics* **2016**, *10*, 585−589.
(30) Xiao, Z.; Tao, T.; Shu, J.; Pan, R.; Dang, W.; Zhao, N.; Pan, S.; Zhang, W. Charge Carrier Recombination Dynamics in MAPb-$(Br_xCl_{1-x})_3$ Single Crystals. *J. Phys. Chem. Lett.* **2023**, *14*, 245−252.
(31) Feng, Y.; Pan, L.; Wei, H.; Liu, Y.; Ni, Z.; Zhao, J.; Rudd, P. N.; Cao, L. R.; Huang, J. Low Defects Density $CsPbBr_3$single Crystals Grown by an Additive Assisted Method for Gamma-Ray Detection. *J. Mater. Chem. C* **2020**, *8*, 11360−11368.
(32) Mix, L. T.; Ghosh, D.; Tisdale, J.; Lee, M.-C.; O'Neal, K. R.; Sirica, N.; Neukirch, A. J.; Nie, W.; Taylor, A. J.; Prasankumar, R. P.; Tretiak, S.; Yarotski, D. A. Hot Carrier Cooling and Recombination Dynamics of Chlorine-Doped Hybrid Perovskite Single Crystals. *J. Phys. Chem. Lett.* **2020**, *11*, 8430−8436.
(33) Khanam, S. J.; Konda, S. R.; Premalatha, A.; Ketavath, R.; Fu, W.; Li, W.; Murali, B. Additive Engineering in $CH_3NH_3PbBr_3$ Single Crystals for Terahertz Devices and Tunable High-Order Harmonics. *J. Mater. Chem. C* **2023**, *11*, 9937−9951.
(34) Han, T.-H.; Lee, J.-W.; Choi, C.; Tan, S.; Lee, C.; Zhao, Y.; Dai, Z.; De Marco, N.; Lee, S.-J.; Bae, S.-H.; Yuan, Y.; Lee, H. M.; Huang, Y.; Yang, Y. Perovskite-Polymer Composite Cross-Linker Approach for Highly-Stable and Efficient Perovskite Solar Cells. *Nat. Commun.* **2019**, *10*, 520.
(35) Shi, D.; Adinolfi, V.; Comin, R.; Yuan, M.; Alarousu, E.; Buin, A.; Chen, Y.; Hoogland, S.; Rothenberger, A.; Katsiev, K.; Losovyj, Y.; Zhang, X.; Dowben, P. A.; Mohammed, O. F.; Sargent, E. H.; Bakr, O. M. Low Trap-State Density and Long Carrier Diffusion in Organolead Trihalide Perovskite Single Crystals. *Science* **2015**, *347* (6221), 519−522.
(36) Juarez-Perez, E. J.; Ono, L. K.; Maeda, M.; Jiang, Y.; Hawash, Z.; Qi, Y. Photodecomposition and Thermal Decomposition in Methylammonium Halide Lead Perovskites and Inferred Design Principles to Increase Photovoltaic Device Stability. *J. Mater. Chem. A* **2018**, *6*, 9604−9612.
(37) Farrukh, M. A.; Butt, K. M.; Chong, K.; Chang, W. S. Photoluminescence Emission Behavior on the Reduced Band Gap of Fe Doping in CeO_2-SiO_2 Nanocomposite and Photophysical Properties. *J. Saudi Chem. Soc.* **2019**, *23*, 561−575.
(38) Zhang, L.; Liu, Y.; Ye, X.; Han, Q.; Ge, C.; Cui, S.; Guo, Q.; Zheng, X.; Zhai, Z.; Tao, X. Exploring Anisotropy on Oriented Wafers of $MAPbBr_3$ Crystals Grown by Controlled Antisolvent Diffusion. *Cryst. Growth Des.* **2018**, *18*, 6652−6660.
(39) Yang, B.; Ming, W.; Du, M.-H.; Keum, J. K.; Puretzky, A. A.; Rouleau, C. M.; Huang, J.; Geohegan, D. B.; Wang, X.; Xiao, K.; Perovskites Yang, O. B.; Yang, B.; Keum, J. K.; Puretzky, A. A.; Rouleau, C. M.; Geohegan, D. B.; Xiao, K.; Ming, W.; Du, M.; Wang, X.; Huang, J. Real-Time Observation of Order-Disorder Transformation of Organic Cations Induced Phase Transition and Anomalous Photoluminescence in Hybrid Perovskites. *Adv. Mater.* **2018**, *30*, 1705801.
(40) Hirori, H.; Xia, P.; Shinohara, Y.; Otobe, T.; Sanari, Y.; Tahara, H.; Ishii, N.; Itatani, J.; Ishikawa, K. L.; Aharen, T.; Ozaki, M.; Wakamiya, A.; Kanemitsu, Y. High-Order Harmonic Generation from Hybrid Organic−Inorganic Perovskite Thin Films. *APL Mater.* **2019**, *7*, 041107.
(41) Nakagawa, K.; Hirori, H.; Sanari, Y.; Sekiguchi, F.; Sato, R.; Saruyama, M.; et al. Interference Effects in High-Order Harmonics from Colloidal Perovskite Nanocrystals Excited by an Elliptically Polarized Laser. *Phys. Rev. Mater.* **2021**, *5*, 016001.
(42) Konda, S. R.; Soma, V. R.; Ganeev, R. A.; Banavoth, M.; Ketavath, R.; Li, W. Third-Order Optical Nonlinearities and High-Order Harmonics Generation in Ni-Doped $CsPbBr_3$ Nanocrystals Using Single- and Two-Colour Chirped Pulses. *J. Mater. Sci.* **2022**, *57*, 3468−3485.
(43) Konda, S. R.; Soma, V. R.; Banavoth, M.; Ketavath, R.; Mottamchetty, V.; Lai, Y. H.; Li, W. High Harmonic Generation from Laser-Induced Plasmas of Ni-Doped $CsPbBr_3$ Nanocrystals: Implications for Extreme Ultraviolet Light Sources. *ACS Appl. Nano Mater.* **2021**, *4*, 8292−8301.

https://doi.org/10.1021/acs.jpclett.3c02454
J. Phys. Chem. Lett. 2023, 14, 9222−9229